 CMES, vol.11, no.2, pp.73-80, 2006

Discrete Dislocation Dynamics Simulation of Interfacial Dislocation Network in Gamma/Gamma-Prime Microstructure of Ni-based Superalloys

K. Yashiro[1], Y. Nakashima[1] and Y. Tomita[1]

Abstract: A simple back force model is proposed for a dislocation cutting into γ' precipitate, taking the work for making and recovering an anti-phase boundary (APB) into account. The first dislocation, or a leading partial of a superdislocation, is acted upon by a back force whose magnitude is equal to the APB energy. The second dislocation, or a trailing partial of a superdislocation, is attracted by the APB with a force of the same magnitude. The model is encoded in the 3D discrete dislocation dynamics (DDD) code and applied to the cutting behavior of dislocations at a γ/γ' interface covered by an interfacial dislocation network. Dislocations are generated from Frank-Read sources and approach the interface. The first dislocation piles up at the interface not by the stress field of the network but by the back force against making an APB. The second dislocation, however, stands off from the interface by the stress field of the first dislocation and the dislocation network. The finer mesh of the network, the further the second dislocation piles up. These two dislocations cut into the precipitate forming a superdislocation under the force from follow-on dislocations. It is also clarified that the penetration takes place from the interspace of the network.

keyword: Discrete Dislocation Dynamics, Anti-Phase Boundary, Ni-Based Superalloys, Interfacial Dislocation Network

1 Introduction

Single crystalline nickel-based superalloys are most prospective materials to improve the heat efficiency of gas turbine engines and aeroengines [Nakagawa (2004)]. They have a characteristic microstructure in which cuboidal γ' phases are precipitated in the γ matrix. The size of the precipitates is precisely controlled to aquire the highest heat tolerance; the typical length of a cuboidal precipitate is less than 0.5 μm and the width of the γ matrix is decreased to a few tens of nanometer in fourth- and higher-generation superalloys. The great heat tolerance of superalloys is attributed to the blocking of free motion of dislocations by the precipitated γ' phases. In addition, the γ' phases change their shape from ultra-fine cubes to coarse plates by aggregating under creep deformation. The plates align normal or parallel to the loading direction depending on the lattice misfit between γ and γ' phases. This coarsening process is referred as rafting [Pollock and Argon (1992)]. The creep resistance increases by the rafting since the rafted γ' plates interrupt dislocations. In addition, network-like dislocations are found on surfaces of the rafted γ' plates in the fourth-generation superalloys and reported to affect the creep resistance [Zhang (2002, 2003)]. Thus the interaction between the γ' phases and dislocations is indispensable for deformation behavior of the superalloys.

We have conducted several molecular dynamics (MD) simulations to determine the fundamental aspect of dislocations at the γ/γ' interface [Yashiro (2002, 2004a)]. MD simulations, however, cannot treat collective behavior of many dislocations nor thermally activated motions such as a dislocation climb. Thus we are now scaling up our study using discrete dislocation dynamics (DDD) simulation [Yashiro (2004b, 2005)]. In the present study, the γ' cutting of dislocations with or without an interfacial dislocation network is investigated by DDD simulations. First we derive the back force acting on dislocations cutting into a γ' phase from the work for making and recovering an anti-phase boundary (APB). This back force model is encoded in the 3D-DDD code proposed by Zbib and coworkers (1998, 2002), and applied to the dislocations approach a flat γ/γ' interface with and without a dislocation network. The mesh of the net is changed to evaluate the cutting resistance of the interfacial dislocation network quantitatively. The APB energy adopted is calculated by *ab-initio* analysis based on the density functional theory (DFT).

[1] Kobe Univ., 1-1, Rokkodai, Nada Kobe JAPAN.

2 Simulation Procedure

2.1 DDD Outline

According to the formulation proposed by Zbib and coworkers (1998, 2002), all dislocation lines and loops of arbitrary shapes are discretized into short line segments and the time evolution of each dislocation is determined by calculating the motion of all nodes. Discretization is updated continuously to represent the arbitrary shapes of dislocations. The force acting on node i of the position vector $\mathbf{p}$ is calculated using

$$\mathbf{F}_i = \sum_{j=1}^{N-1} \left(\sigma^D_{j,j+1}(\mathbf{p}) + \sigma^{\mathrm{a}}(\mathbf{p})\right) \cdot \mathbf{b}_i \times \boldsymbol{\xi}_i + \mathbf{F}_{i-\mathrm{self}}, \tag{1}$$

where $\sigma^D_{j,j+1}(\mathbf{p})$ is the stress at $\mathbf{p}$ generated by a remote segment between j and j+1, $\sigma^{\mathrm{a}}(\mathbf{p})$ the applied stress, and N the number of nodes; $\mathbf{b}_i$ and $\boldsymbol{\xi}_i$ are the Burgers vector and line sense vector at node i, respectively, as shown in Fig.1. Thus the first term on the right-hand side of Eq. (1) represents the Peach-Koehler (PK) force. $\mathbf{F}_{i-self}$ is the line tension evaluated by the curvature at node i. The motion of dislocations is traced by solving the following equation of motion numerically.

$$m\dot{\mathbf{v}}_i + \frac{1}{M(T,p)}\mathbf{v}_i = [\mathbf{F}_i]_{\mathrm{slip-direction}}. \tag{2}$$

Here, $\mathbf{v}_i$ is the glide velocity and m the effective mass per unit dislocation; T and p are the temperature and pressure, respectively. M is the mobility accounting for damping effects, such as phonon drag. In the present study, m and M are set to $\rho b^2/2$ and $10^{-2}\,(\mathrm{Pa.s})^{-1}$, respectively, where ρ is the density.

2.2 DDD-FEM Coupling

The formulation of $\sigma^D_{j,j+1}(\mathbf{p})$ is defined in the infinite body of a homogeneous material, so that it could not directly be applied to solving the problem regarding surfaces or heterogeneous interfaces. The superposition principle is used to treat the problem. The displacement $\mathbf{u}$, strain ε, and stress σ in a finite body containing γ' phase is given by the sum of the two solutions

$$\mathbf{u} = \mathbf{u}^\infty + \mathbf{u}^*, \quad \varepsilon = \varepsilon^\infty + \varepsilon^*, \quad \sigma = \sigma^\infty + \sigma^*, \tag{3}$$

where ∞ implies the solution of DDD analysis for the domain V in an infinite homogeneous body, while * that

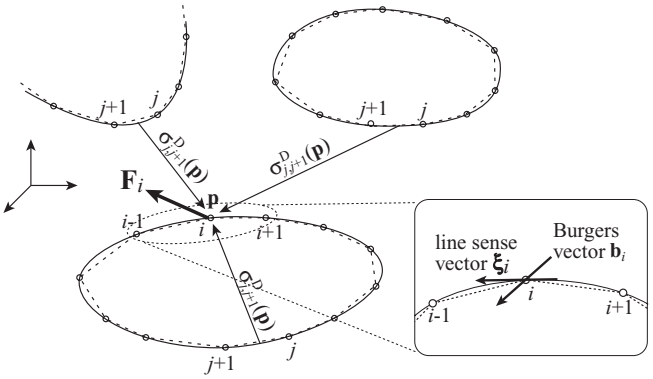

Figure 1 : Nodes and segments on dislocation loops.

of FEM for a finite body with a volume V. In the FEM analysis, the following constitutive equations are defined for the matrix and precipitate, respectively.

$$\begin{array}{ll} \text{In matrix:} & \sigma^* = [C_{\mathrm{m}}]\varepsilon^* \\ \text{In precipitate:} & \sigma^* = [C_{\mathrm{p}}]\varepsilon^* + [C_{\mathrm{p}} - C_{\mathrm{m}}]\varepsilon^\infty \end{array} \tag{4}$$

Here, C_{m} and C_{p} are the elastic stiffnesses of the matrix and precipitate, respectively. The second term of the lower equation is the "eigenstress". The boundary conditions are

$$\mathbf{t}^* = \mathbf{t}^{\mathrm{a}} - \mathbf{t}^\infty \tag{5}$$

$$\mathbf{u}^* = \mathbf{u}^\infty \tag{6}$$

where $\mathbf{t}^{\mathrm{a}}$ is the externally applied traction while $\mathbf{t}^\infty$ is the traction caused by dislocations resulting from the infinite-homogeneous-domain problem.

2.3 Back Force Condition

When a dislocation cuts into or glides in a γ' precipitate, it leaves an anti-phase boundary on the slip plane. Thus, an excess energy equal to the APB energy of the swept area is necessary to cut into or move in the precipitate. Consider a straight segment of L length that travels normal to the segment at a distance n. The APB energy of the swept area is expressed as

$$E_{\mathrm{APB}} = \chi_{\mathrm{APB}} L n \tag{7}$$

where χ_{APB} is the inherent APB energy per unit area. A dislocation should cut into the precipitate against the repulsive force, or "back-force", due to the APB energy. Assume that the back force on dislocation is constant in

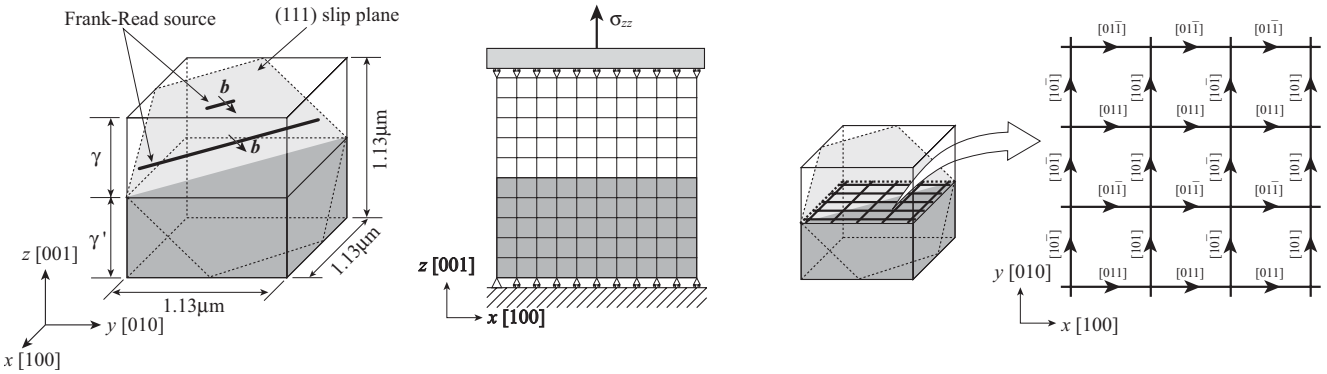

(a) Dimensions of simulation cell (b) Loading condition and FEM mesh (c) Burgers vectors of interfacial dislocation network

Figure 2 : Simulation model and conditions.

the precipitate. Then the work done by the dislocation is written as

$$W = F_{\mathrm{b}} L n \tag{8}$$

where F_{b} is the back force per unit length. Assuming that all the work converts energy increase, *e.g.* $W = E_{\mathrm{APB}}$, we obtain $F_{\mathrm{b}} = \chi_{\mathrm{APB}}$. The unit of the energy per area is converted to that of force per length as J/m^2=Nm/m^2=N/m. When the next position of a dislocation node i is in the area of γ' precipitate, or the dislocation expands the APB, the node receives a repulsive force of F_{b}. On the other hand, the follow-on dislocation gliding in the APB receives an attractive force of F_{b} to dissolve the APB.

2.4 Simulation Model

The back force condition is encoded in the DDD-FEM simulation package, that is, multiscale dislocation dynamics plasticity (MDDP), developed by Zbib and coworkers (1998, 2002). All the short-range interactions of dislocations, such as annihilation, junction and jog formation, are included in the DDD package. As shown in Fig. 2, a cubic cell made of γ and γ' layers is used in this study. The cell is 1.13 μm in length and each of its layer has the same thickness of 0.57 μm. The shear moduli of the γ and γ' phases are set to 80GPa and 85GPa, respectively. Poisson's ratio is set to 0.3 for both phases. Two Frank-Read (FR) sources whose Burgers vector is $[01\bar{1}]$ are set on the same (111) slip plane, as schematically shown in the figure. The source near the interface has a width of 1.51 μm (6040b, b is the magnitude of Burgers vector) while the other source 0.21 μm (800b). To accelerate the propagation of dislocation loops and bring dislocations to the interface, a uniform stress of 550MPa is applied in the z-direction in the DDD analysis. In the FEM analysis, the cell is divided into $10 \times 10 \times 10$ cubic elements and subjected to the loading conditions shown in Fig. 2(b). Here, the periodic boundary condition tends to significantly multiply dislocations and easily reaches the computational limit, so that we adopt the free boundary condition in which dislocations receive the image force near the surface. With these conditions, we first simulate the dislocation behavior at a flat γ/γ' interface without dislocation network. Then we arrange the dislocation network on the γ/γ' interface, as schematically shown in Fig. 2(c), and perform the DDD simulation in the same way. Here the mesh spacing of $d = 0.226\,\mu$m, 0.126 μm and 0.075 μm are considered for the network, respectively. The Burgers vectors of the network dislocations are defined experimentally as shown in Fig. 2(c). It is also revealed that the intersections have different Burgers vectors [Zhang (2002)], however, we simplify the network have no intersection but overpasses. The slip plane of the FR source crosses just at these overpasses of the dislocation network.

The APB energy χ_{APB} is set to 126 mJ/m^2 in all the simulations. The energy is evaluated using the Vienna ab-initio simulation program [Kresse and Hafner (1993)] with ultrasoft pseudopotential and generalized gradient approximation (GGA). 2, 4 and 8 unit lattices of Ni_3Al are stacked as supercells and two APB planes are introduced in the supercells. Then χ_{APB} is evaluated by the energy increase of these supercells from the reference energy of a perfect single crystal. $\boldsymbol{k}$-points of $8 \times 8 \times 3$ and a cutoff energy of 241.62eV are used in the calculations.

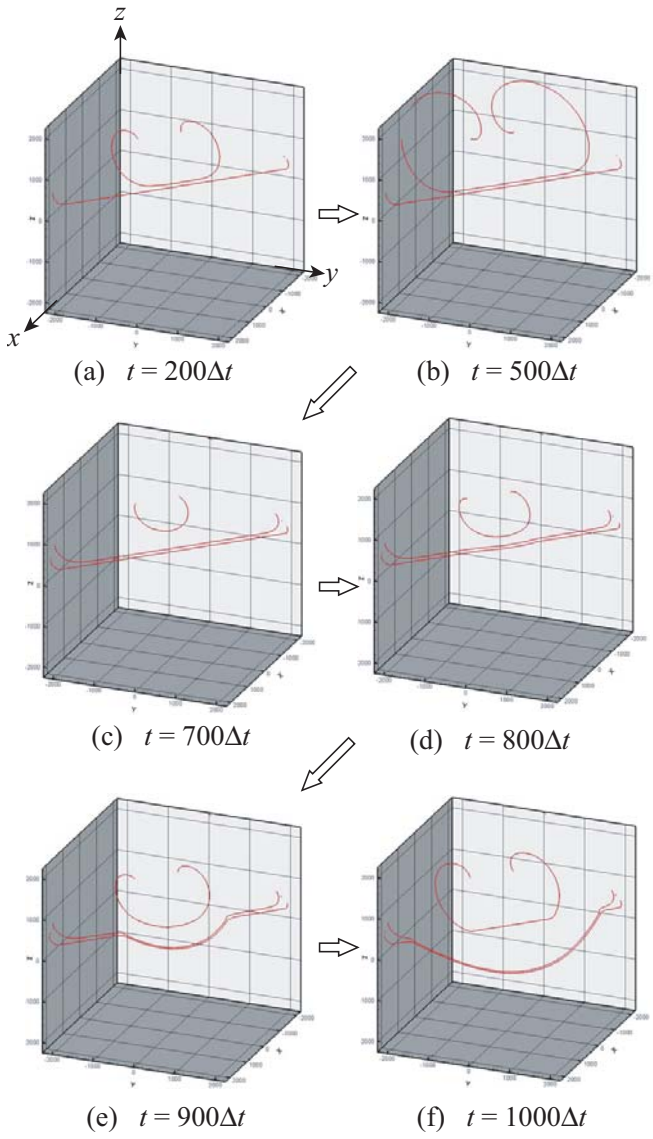

Figure 3 : Motion of dislocations at a flat γ/γ' interface (without dislocation network).

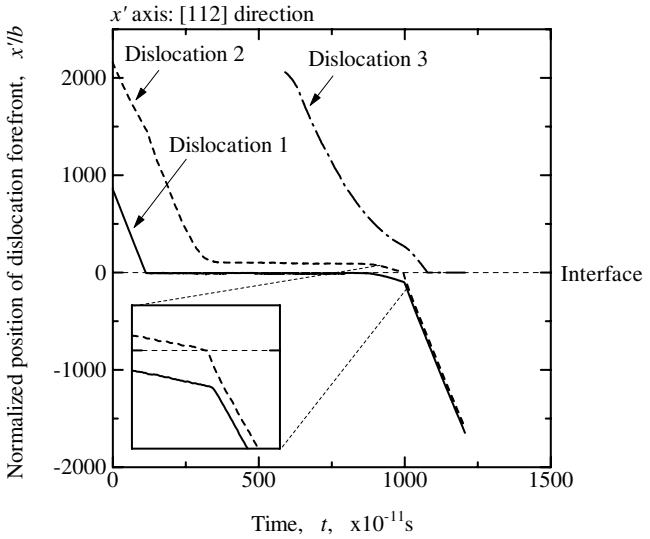

Figure 4 : Normalized position of dislocation forefront (without dislocation network).

3 Result and Discussions

3.1 Dislocation Motion at Plain Interface

Figure 3 shows the dislocation motion at the γ/γ' interface *without* interfacial dislocation network. There is the γ' phase in the lower half of the cell although it is not indicated in the figure. The time increment $\Delta t = 10^{-11}$s is used in the numerical integration of Eq. (2), to capture the dislocation behavior at the interface correctly as well as the short-range interaction, *e.g.* annihilation. The first dislocation from the longer FR source piles at the interface quickly. The second dislocation that propagates from the shorter FR source is also blocked at the interface by the repulsive force from the first dislocation, and straightened along the interface during $t = 200 \sim 500\Delta t$. The pair of these dislocations, however, cannot penetrate into the γ' phase at this stage despite an applied external stress of σ_{zz} = 550MPa. When the third dislocation is generated by multiplication at the shorter FR source and approaches the dislocation pair, the pair begin to cut into the γ' phase and form a superdislocation (t = 800 $\sim$ 900Δt). Once the superdislocation nucleates, it goes through the γ' phase as fast as the dislocations in the γ phase since the repulsive and attractive back forces cancel out each other and the shear moduli of both phases are almost same. The superpartials maintain a constant distance in the γ' phase and their width is about 13nm ($52b$). The third dislocation piles at the interface again in Fig. 3(f) of $t = 1000\Delta t$. This motion of dislocations is quantitatively indicated in Fig. 4. The abscissa is the time step, and the ordinate the distance from the interface evaluated at the forefront of dislocation loops. The first and second dislocations pile at the interface and maintain a constant distance until the third dislocation approaches. Then the first dislocation cuts into the γ' phase at about $t = 900\Delta t$ and the second approaches the interface while keeping its distance to the first dislocation. During this penetration, the velocity of two dislocations is low since

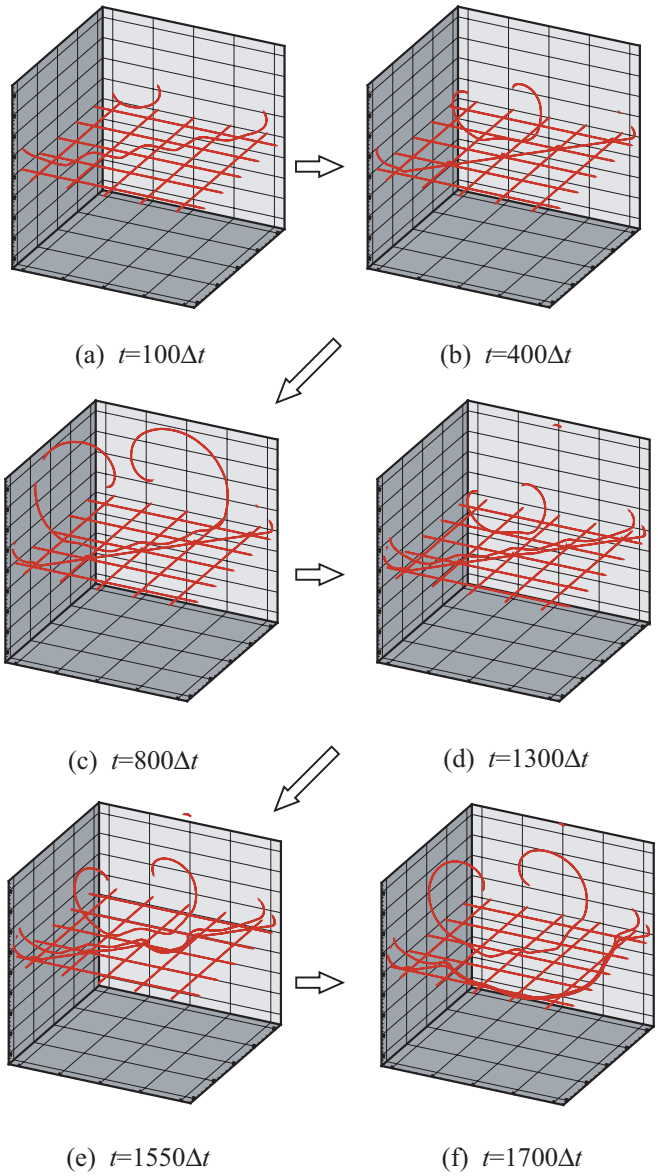

Figure 5 : Cutting of interfacial dislocation network with the net spacing of $d = 0.226\,\mu$m.

the back force of the APB acts only on the first dislocation. That is, in our model, the APB does not generate an attractive force on the trailing dislocation away from the interface, and expands larger than the equilibrium width in the nucleation of a superdislocation. This phenomenon, however, does not conflict with our MD results in which the APB does not attract a trailing dislocation [Yashiro (2002)]. When the second dislocation reaches the interface, it receives an attractive force from the APB and increases its velocity, resulting in the decrease in the width of superpartials. The superdislocation

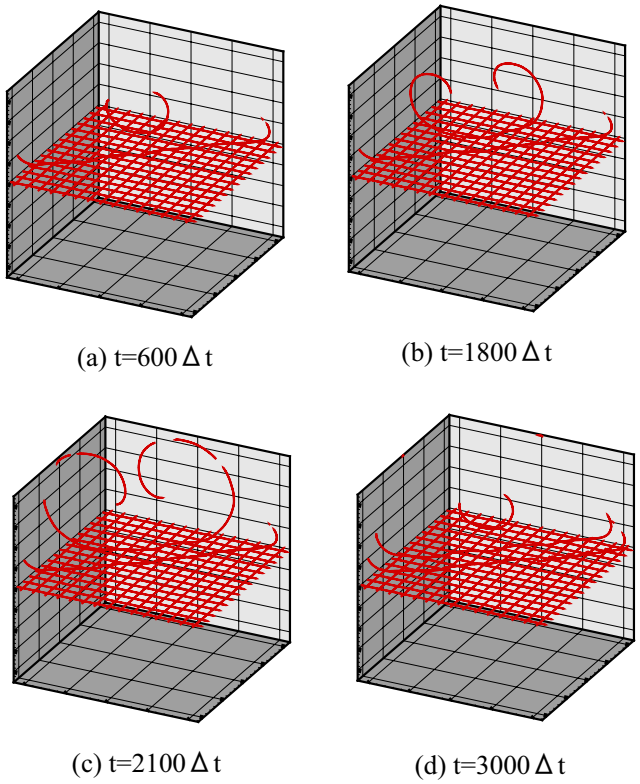

Figure 6 : Slowdown of the dislocations near the network dislocations with the net spacing of $d = 0.075\,\mu$m.

glides swiftly in the γ' phase when the trailing superpartial catches up with the leading dislocation and reaches the equilibrium distance in which back forces cancel out.

3.2 Dislocation Cutting of Interfacial Dislocation Network

Figure 5 shows the dislocation motion near the γ/γ' interface covered by the network dislocations with the mesh spacing of $d = 0.226\,\mu$m. In Fig. 5(a) of $t = 100\Delta t$, the first dislocation vacillates due to the stress field of the network. Then the dislocation is pressed to the interface and straightened in the interspace of the network, however, the overpasses prevent it from approaching the interface (Fig. 5(b)). The second dislocation becomes more wavy at these overpasses as shown in Figs. 5(c) and (d). The dislocations cut into the γ' phase from the interspace of the dislocation net after they are pinned at the overpasses and bowed-out as shown in Figs. 5(e) and (f). In the simulation of $d = 0.126\mu$m, the superdislocation also nucleates from the interspace while the penetration does not take place until the fourth dislocation is multiplied

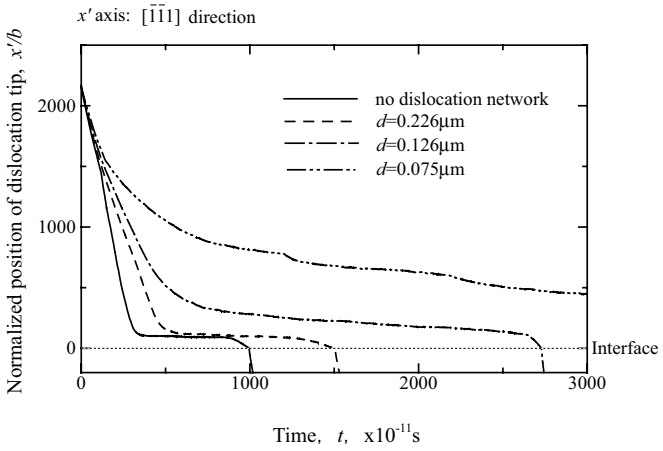

Figure 7 : Normalized position of the tip of second dislocation.

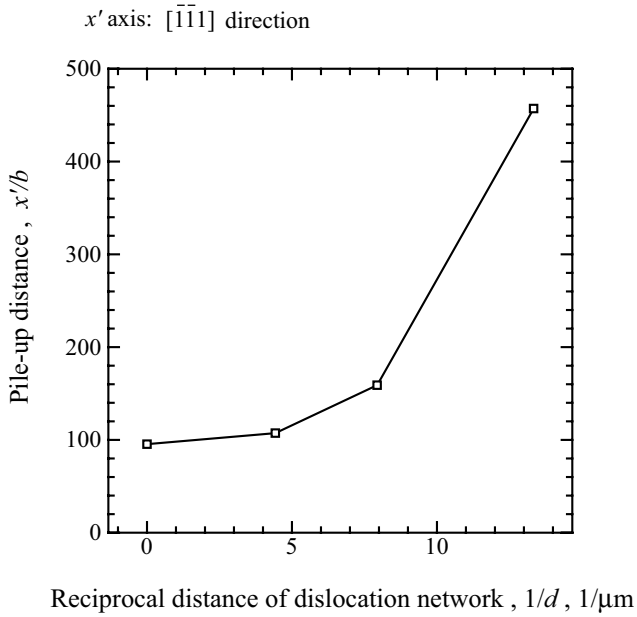

Figure 8 : Change in the pile-up distance with the net spacing.

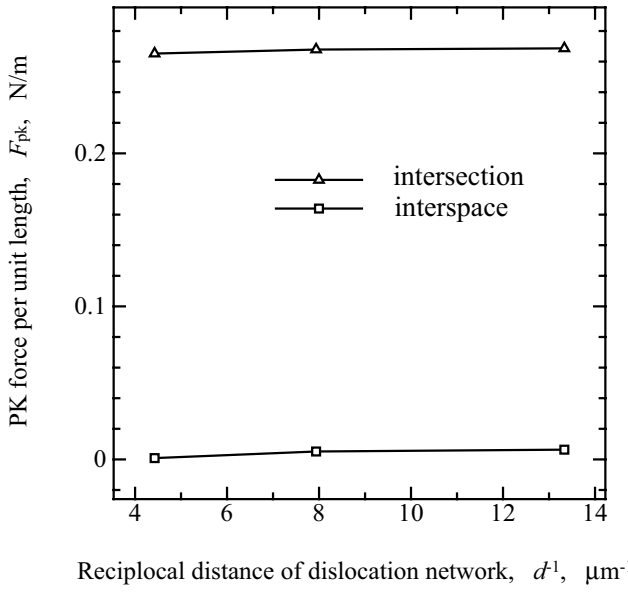

Figure 9 : Peach-Koehler force measured in the vicinity of dislocation network.

at the shorter FR source. On the other hand, the dislocations cannot cut into the γ' phase during the simulation time of $3000\Delta t$ in the simulation of $d = 0.075\mu$m as shown in Fig. 6, since the second dislocation is kept far away from the interface and prevents the third dislocation from propagation.

The change in the tip position of the second dislocation loop is evaluated in all simulations and summarized in Fig. 7. The abscissa is time step; the ordinate is the distance from the interface evaluated at the tip of dislocation loops. There is no large difference in the pile-up position between the simulation of $d = 0.226\,\mu$m and that without dislocation network, however, the second dislocation of the former simulation reaches there in delay against the latter. The pile-up position is about 24nm from the interface. The second dislocation slowly accesses to the interface in the simulation of $d = 0.126\,\mu$m. The distance between the second dislocation and the interface is about 40nm when the superdislocation nucleates in the simulation of $d = 0.126\,\mu$m. On the other hand, the second dislocation hardly approaches the interface and remains the distance of about 115nm even at $t = 3000\Delta t$ in the simulation of $d = 0.075\,\mu$m.

3.3 Cutting Resistance of Dislocation Network

The pile-up position of the second dislocation above mentioned is summarized in Fig. 8. The abscissa is the reciprocal of the net spacing, d^{-1}; the ordinate is the pile-up position from the γ/γ' interface. The result of the simulation without interfacial dislocation is also shown as d^{-1}=0. The deposition of the second dislocation becomes exponentially further from the interface with the reciprocal of net spacing.

To discuss the cutting resistance more quantitatively, the PK force acting on a dislocation node is evaluated at the center of interspace and at the overpass, respectively.

Figure 9 shows the magnitude of the force which is measured for an ideal dislocation line located at a distance of $10b$ from the γ/γ' interface. The repulsive back force of the APB, F_b=0.126 N/m, is not included since the measurement is done slightly away from the interface. The dislocation receives back force of about 0.27N/m, twice large as F_b, at the overpass. On the other hand, the back force is almost zero at the center of the interspace. Thus the dislocation penetrates into the γ' phase from the interspace. Here, it is noteworthy that these back forces are almost constant against the mesh spacing. That is, the stress field of a dislocation network does not change the local cutting resistance while it puts off the remote dislocation drastically as shown in Fig. 8. The finer mesh of the network, the greater force the dislocation needs to bow out in the interspace due to the line tension. In the present simulations, the remote effect of the stress field might be overestimated since the dislocation network is not composed of misfit dislocations but those in the γ' phase; however, the cutting resistance will still increase according to the mesh spacing due to the pinning and bow-out by the dislocation network.

4 Conclusion

To simulate dislocation behavior at the γ/γ' interface, a back force model for discrete dislocation dynamics (DDD) simulation is proposed according to the work for making/recovering an anti-phase boundary (APB). We first evaluate the APB energy of 126 mJ/m^2 by *ab-initio* calculation based on the DFT-GGA (density functional theory - generalized gradient approximation) ultrasoft pseudopotential method. The APB energy is encoded in the DDD simulation package as a back force condition. It is demonstrated that a superdislocation nucleates after two dislocations pile up at a plane γ/γ' interface and that the width of superpartials is naturally balanced by the APB energy and repulsion of dislocations. Then the interfacial dislocation network is set on the γ/γ' interface changing the mesh spacing to investigate the cutting resistance quantitatively. The stress field of the network puts off remote dislocations from the network exponentially with the reciprocal of the mesh spacing while it does not change the local cutting resistance of the network. The dislocation network in real superalloys, which is composed of misfit dislocations, would have weaker stress field; however, the cutting resistance will increase with the decrease in the mesh spacing since dislocations need greater force to bow out in the interspace due to the line tension.

Acknowledgement: This work was supported financially in part by a Grant-in-Aid for Scientific Research from the Ministry of Education, Culture, Sports, Science and Technology of Japan.

References

Kresse, G.; Hafner, J. (1993): Ab Initio Molecular Dynamics for Liquid Metals. *Phys. Rev.* B, vol.47, pp.558–561.

Nakagawa, Y. (2004): Aero-engine business and material technologies in Japan. In: Green, K. A. et al. (ed) *Superalloys 2004*, TMS, pp.3–12.

Pollock, T. M.; Argon, A. S. (1992): Creep resistance of CMSX-3 nickel base superalloy single crystals. *Acta Metal. Mater.*, vol.40, pp.1–30.

Yashiro, K.; Naito, M.; Tomita, Y. (2002): Molecular Dynamics Simulation of Dislocation Nucleation and Motion at γ/γ' Interface in Ni-Based Superalloy. *Int. J. Mech. Sci.*, vol.44, pp.1845–1860.

Yashiro, K.; Tabata, Y.; Tomita, Y. (2004a): Molecular Dynamics Study on the Characterisitics of Edge and Screw Dislocations in Gamma/Gamma-Prime Microstructure in Ni-based Superalloy. In: Kitagawa, H. and Shibutani, Y. (ed) *IUTAM Symposium on Mesoscopic Dynamics of Fracture Process and Material Strength*, pp.59–68.

Yashiro, K.; Tabata, Y.; Kurose, F.; Tomita, Y.; Zbib, H. M. (2004b): MD / DDD Study on Dislocation Behaviors at Matrix-Precipitate Interface in Nickel-Based Superalloys. *MMM-II Conference Proceedings*, pp.169–172.

Yashiro, K.; Tabata, Y.; Kurose, F.; Tomita, Y.; Zbib, H. M. (2005): Discrete Dislocation Dynamics Simulation of Cutting of γ' Precipitate and Interfacial Dislocation Network in Ni-Based Superalloys. *Int. J. Plasticity*, in press.

Zbib, H. M.; Rhee, M.; Hirth, J. P. (1998): On Plastic Deformation and the Dynamics of 3D Dislocations. *Int. J. Mech. Sci.*, vol.40, pp.113-127.

Zbib, H. M.; Diaz de la Rubia, T. (2002): A multiscale model of plasticity. *Int. J. Plasticity*, vol.18, pp.1133–1163.

Zhang, J. X.; Murakumo, T.; Koizumi, Y.; Kobayashi, T.; Harada, H.; Masaki Jr. S. (2002): Interfacial dislocation networks strengthening a fourth generation single-crystal TMS-138 superalloy. *Metal. Mater. Trans.*, vol.33A, pp.3741–3746.

Zhang, J. X.; Murakumo, T.; Koizumi, Y.; Harada, H. (2003): The influence of interfacial dislocation arrangements in a fourth generation single crystal TMS-138 superalloy on creep properties, *J. Mater. Sci.*, vol.38, pp.4883–4888.